Journal of Renewable Energy and Environment

Research Article

Journal Homepage: www.jree.ir

A Study on the Kinetics and Effects of three Combustion Fuels on Retort Carbonization of Corn Husk and Cob

Mubarak A. Amoloye[1], Sulyman. A. Abdulkareem[1], Adewale George Adeniyi[1*]
[1]*Department of Chemical Engineering, University of Ilorin, P. M. B. 1515, Ilorin, Nigeria*

P A P E R I N F O

Paper history:
Received ?? ??????? 2020
Accepted in revised form ?? ????? 2020

Keywords:
Coats-Redfern
Biochar
TGA
Kinetic Models

A B S T R A C T

The drive to move away from fossil fuels and related products has drawn significant attention to biomass and biomass-related products in recent times. This study reports the effect of three forest biomass sources namely *acacia auriculiformis*, *terminalia randii*, and *delonix regia* as combustion fuels in a retort heated, low-temperature and top-lit updraft gasifier on biochars produced from two agricultural wastes: corn husk and corn cob. The combustion fuels were characterized using Thermogravimetric/Differential thermogravimetric analysis. Their TGA data were fitted to 16 kinetic models using the Coats-Redfern method. Characterization of the products was performed using Scanning Electron Microscopy/Energy Dispersive X-ray Spectroscopy and Fourier Transform Infra-Red Spectroscopy. Results revealed similar decomposition trends for combustion fuels. Different kinetic models predicted decomposition mechanisms of combustion fuels for the regions considered. Negative correlation was found between biochar yields and increasing carbonization temperatures with yields ranging from 64.6-37.8 % and 28.4-24.5% for corn husk and cob, respectively. Results indicate similar effects of combustion fuels on functional groups contained in biochar samples.

Doi:https://doi.org/10.30501/jree.2023.387471.1557

1. INTRODUCTION

The ever-growing global population and increased anthropogenic activities have created a pressing need to meet global energy demand and ensure global food security (Panwar et al., 2019). Over the years, fossil fuels (natural gas, coal, and crude oil) have continued to be the dominant source of energy supply in the world. However, finding solutions to the challenges posed by the increasing energy demand, diminishing fossil fuel reserves, and the search for sustainable and environmentally friendly alternatives have been the primary focus of research in recent years. The dependence on fossil fuels as a major source of energy has had detrimental effects on the climate due to greenhouse gas emissions, causing global warming (Santos & Alencar, 2019; Sarkar et al., 2014; Zecca & Chiari, 2010)
. In addition, in order to meet the global demand for food, growing activities in the agricultural sector demand making efforts to mitigate the environmental impacts of improper disposal of agricultural wastes on the environment (Panwar et al., 2019). Luckily, the utilization of biomass such as forest and agricultural wastes for biofuel(s) production has not only introduced a promising alternative to the use of fossil fuels, but also concurrently provided a means of reducing the environmental impacts of the improper disposal of these wastes on the environment. Biofuel production through thermochemical technologies such as pyrolysis, gasification, carbonization, etc. has proven efficient for harnessing numerous benefits in biomass. Among the benefits of subjecting biomass to thermochemical processes is the production of biochar, a carbon-concentrated solid product. There have been numerous research works reported and ongoing on biochar production from various biomass sources, primarily due to its numerous ecological (Ghani et al., 2013; Kajina & Rousset, 2018; Leeq et al., 2010)
, economic (Hildago-oporto et al., 2019; Liu et al., 2019; Zhou et al., 2016)
, and environmental (Adeniyi et al., 2022)
benefits. Even though raw materials for biochar production are more or less free, commercialization of its production is, in fact, capital-intensive. Therefore, increased efforts have been made to develop local technologies for biochar production, especially in developing countries and specifically Nigeria. This is particularly important as the country faces challenges with inconsistent power supply and escalating costs. Recently, several studies have already addressed the issue of biomass carbonization for biochar production with a retort heating system, which involves the utilization of biomass (waste forest biomass sources) as combustion fuels. Adeniyi et al. (2019b) reported the production of biochar from elephant grass using a fabricated low-temperature, top-lit updraft gasifier (TLUG) with the stems and stalks of *Bambusa vulgaris* and *Daniellia olivieri* as combustion fuels. Similarly, the use of the aforementioned combustion fuels was also employed for the production of biochar from plantain fibers in another study (Adeniyi et al., 2019a). Few other studies that have employed similar concepts like the ones mentioned earlier for biochar production include the co-carbonization of sugarcane bagasse/low density polyethylene wastes (Adeniyi et al., 2020) (LDPE), co-carbonization of dry almond leaves/LDPE, co-carbonization of corn cob/LDPE (Amoloye et al., 2023), and co-carbonization of corn husk/LDPE Amoloye et al., 2022). Until now, the emphasis has been primarily on the resulting product of the carbonization process, namely biochar, with little attention given to the combustion fuel itself. However, it is crucial to recognize that the combustion fuel plays a vital role as it provides the essential heat required for the carbonization process. These combustion fuels enjoy different thermal properties, which could invariably affect the quantity and quality of the biochar produced. To the best of authors' knowledge, no study has been reported on the thermal stabilities/properties and estimation of kinetic parameters of the thermal decomposition of the combustion fuels used in earlier reports. Such information may be necessary for reactor design and process system optimization purposes. Therefore, the aim of this study was to investigate the effects of three different forest biomass sources used as combustion fuels in a TLUG on the temperature profiles, yields, and product qualities of biochars produced from two different corn residues (agricultural wastes). This study elucidates the thermal properties of some waste forest biomass and emphasizes their utilities as sources for heat generation. Further, the utilization of both forest and agricultural wastes justifies the need to find value for waste materials.

2. EXPERIMENTAL

2.1 Thermogravimetric (TG) Analysis of Combustion Fuel Samples

Samples of combustion fuels were sourced from the waste stalks and stems of three different trees, namely *acacia auriculiformis* (northern black wattle), *terminalia randii* (flora of Zimbabwe), and *delonix regia* (flamboyant). Samples were labeled A, B, and C

*Corresponding Author's Email: adeniyi.ag@unilorin.edu.ng

URL: https://www.jree.ir/article_176482.html

for ease of identification. A known amount of samples (15.103 mg of A; 14.338 mg of B; and 13.617 mg of C) underwent thermogravimetric analysis TGA/SDTA85. The samples were heated from 30 °C to 900 °C at a constant and low heating rate of 10°C/min, with a constant supply of N_2 gas to maintain an inert atmosphere.

2.2 Kinetic Analysis

The thermal decomposition of biomass usually involves devolatilization of light volatiles due to decomposition of its constituents as temperature increases, leaving behind the solid products (biochar), and the rate of decomposition is generally represented mathematically as (Rony et al., 2019):

$$\frac{d\theta}{dt} = k(T)f(\theta) \qquad 1$$

The term θ represents the extent of conversion generally expressed as:

$$\theta = \frac{\varepsilon_o - \varepsilon_t}{\varepsilon_o - \varepsilon_f} \qquad 2$$

where $\varepsilon_o$represents the initial mass, ε_t is the mass at time t, and ε_f is the final mass at the end of the thermal decomposition. $k(T)$ is a constant dependent on temperature and expressed by the Arrhenius equation (3). The term $f(\theta)$ is a function describing the path or mechanism of the reaction.

$$k(T) = k_o exp\left(-\frac{E_\theta}{RT}\right) \qquad 3$$

From Equation (3), k_o represents the pre-exponential factor (s^{-1}), E_θ is the activation energy (kJ/mol), R is the universal gas constant (8314J/K.mol), and T (K) is the reaction temperature. Following the steps reported elsewhere (Matali et al., 2020) by substituting (3) into (1), rearranging the equation, and taking the integral within the limits of 0 and T, one can get Equation (4):

$$g(\theta) = \int_0^\theta \frac{d\theta}{f(\theta)} = \frac{k_o}{\beta}\int_0^T \exp[-\frac{E_\theta}{RT}]\, dT = \left(\frac{k_o E_\theta}{\beta R}\right) p(x) \qquad 4$$

where $g(\theta)$ is the integral form of the conversion function, $\beta = \frac{dT}{dt}$ represents the heating rate, and $p(x)$ is the integral form of the temperature term on the right-hand side of (4) which has no exact solution (Santos et al., 2020). There are two main methods for approximating the solution of (4): the iso-conversional model free methods and the model-fitting method. Activation energy E can be well estimated without understanding the reaction mechanism(s) using the model free methods. This is because this method is dependent on weight loss-temperature data of a particular sample at different heating rates for a chosen conversion (Dhaundiyal et al., 2018). The model-fitting method is based on the Coats & Redfern (1964)

Table 1: Selected reaction models for the description of the thermal decomposition of combustion fuels

Model No	Nucleation Models	$g(\theta)$
1	Power Law	$\theta^{\frac{1}{2}}$
2	Power Law	$\theta^{\frac{1}{3}}$
3	Power Law	$\theta^{\frac{1}{4}}$
4	Avrami-Erofeyev	$[-\ln(1-\theta)^{\frac{1}{2}}]$
5	Avrami-Erofeyev	$[-\ln(1-\theta)^{\frac{1}{3}}]$
6	Avrami-Erofeyev	$[-\ln(1-\theta)^{\frac{1}{4}}]$
	Diffusion Models	
7	1-D Diffusion Control	θ^2 $[(1-\theta)\ln(1-\theta)] + \theta$

130
0

8	2D-Diffusion Control	
9	3D-Diffusion Control	$[1-(1-\theta)^{\frac{1}{3}}]^2$
10	Ginstling-Brounshtein 4D-Diffusion Control	$1-\frac{2}{3}\theta-(1-\theta)^{\frac{2}{3}}$
	Reaction order and Geometrical Contraction Model	
11	Zero Order	θ
12	First order	$-\ln(1-\theta)$
13	Second order	$\left[\frac{1}{(1-\theta)}\right]-1$
14	Third Order	$\frac{1}{2}[(1-\theta)^{-2}-1]$
15	Contracting Cylinder	$1-(1-\theta)^{\frac{1}{2}}$
16	Contracting Sphere	$1-(1-\theta)^{\frac{1}{3}}$

asymptotic technique for approximating the integral in (4):

$$\ln\left[\frac{g(\theta)}{T^2}\right]=\ln\left[\frac{k_0R}{\beta E}\right]-\frac{E_\theta}{RT} \quad 5$$

It is convenient to estimate the activation energy, pre-exponential and predict the reaction mechanism by plotting a graph of $\ln\left[\frac{g(\theta)}{T^2}\right]$ against $1000/T$. Several kinetic models were utilized to fit the data, and the model with the best fit was selected. In this study, the Coats-Redfern (C-R) model-fitting method was specifically employed for the kinetic analysis of the combustion fuels. This choice was made since the TG data for these fuels were recorded at a single heating rate. The kinetic models selected are shown in **Table 1**. The models were fitted using OriginPro 2018 and R^2 values were calculated.

3. METHOD

3.1 Brief reactor and reactor temperature profile description

The reactor is comprised of two symmetrically assembled cylinders, with the larger unit referred to as the combustion chamber and the other as the carbonization chamber (see **Figure 1**). The concept was based on a retort heating process where the necessary heat (a key feature) for the thermochemical conversion in the carbonization chamber was provided by the controlled combustion of the fuel used (dried stems and stalks of trees) in the combustion chamber of the reactor.

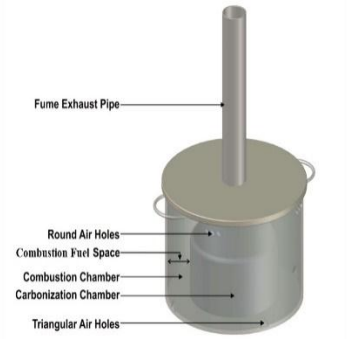

Fig.1: A 3D representation of top-lit updraft gasifier (TLUG)

Further, from previous publications in this area, one major converging characteristic is found in the reactor temperature profile for every batch experiment (**Figure 2**). As can be seen from **Figure 2**, a gradual and steady rise in the temperature of the reactor is observed due to

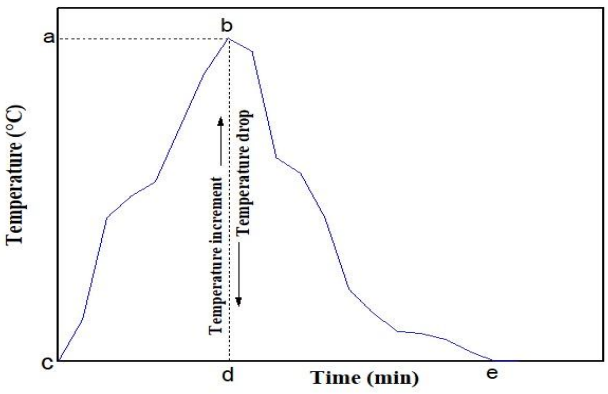

Fig. 2: A typical temperature profile of a carbonization process in a TLUG

continuous partial oxidation of the combustion fuel in the heating gap between the combustion and the carbonization chambers (from point c to a). Then, at point b, a particular maximum temperature is reached (referred to as the peak temperature) after which a perpetual temperature drop is observed (batch carbonization ends at point e). Depending on the thermal properties/capacities of the biomass source employed as the combustion fuel, both peak temperatures and process times could also be affected.

3.3 Batch Carbonization Experiment

The batch experimental procedure used in the study was adapted from (Adeniyi et al., 2019a). The corn residues for the experiments were denoted as corn husk (R1) and corn cob (R2) and the combustion fuels were denoted as A, B, and C. Carbonization chamber was loaded with 16.4 g of R1. The heating space between the combustion and the carbonization chamber was filled with combustion fuel A. The reactor was ignited from the top and allowed to burn in open air for about two minutes. This was done to allow uniformity all around the combustion front at the top of the reactor. Subsequently, the reactor was covered with the lid. Temperature measurements were taken at various points T_a, T_b, T_c, and T_d just before ignition and stopped immediately when the temperature of the system reached equilibrium with ambient conditions. The product (biochar) was removed and weighed; then, the yield was calculated using Equations (6)-(8). The procedure was repeated with R1 and R2 (50 g) using combustion fuels A, B, and C comprising a total of six experimental runs.

$$m_{bio-char} = M_3 - M_2 \quad (6)$$

$$m_{raw} = M_1 - M_2 \quad (7)$$

$$Yield_{bio-char} = \frac{m_{bio-char}}{m_{raw}} \times 100\ \%. \quad (8)$$

where M_1 = mass of the feed chamber + feed (in grams)

M_2 = mass of the feed chamber (in grams)

M_3 = mass of the feed chamber + product

3.2 Product Characterization

The surface morphologies of the particles and elemental analysis of the products were studied using Scanning electron microscopy-Energy dispersive X-ray spectroscopy (SEM-EDS). The acceleration voltage of the microscope was set to 15kV and magnifications of 500 to 1000 times were obtained for the samples. Fourier transform infrared spectroscopy (FTIR) was employed to study the functional groups and complexes present in the samples. The spectra were recorded using transmittance method in the region of 4000–650 cm^{-1} with 30 sample scans.

4. RESULTS AND DISCUSSION

4.1 Thermogravimetric Analysis

Thermal characteristics of combustion fuels A, B, and C were investigated using thermogravimetric analysis (TG) at a constant and low heating rate (10 °C/min). Low heating rates are known to provide a better description of the pyrolytic characteristics of materials, as they allow for improved heat transfer efficiency from the surface to the core of the materials (Rony et al., 2019; Santos et al., 2020)

The samples were heated from 30 °C to 900 °C in an inert atmosphere. The mean normalized sample mass for individual biomass considered is expressed as a function of temperature in the

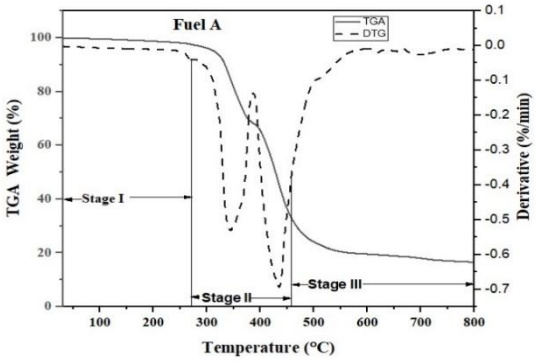

Figure 3. TGA/DTG curves of Combustion Fuel A

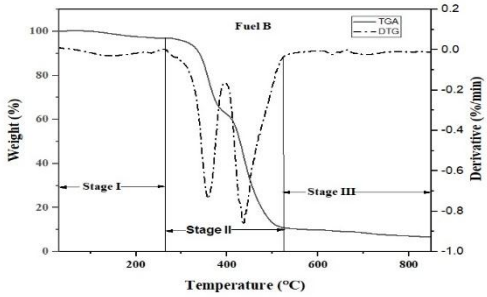

Figure 4. TGA/DTG curves of Combustion Fuel B

130

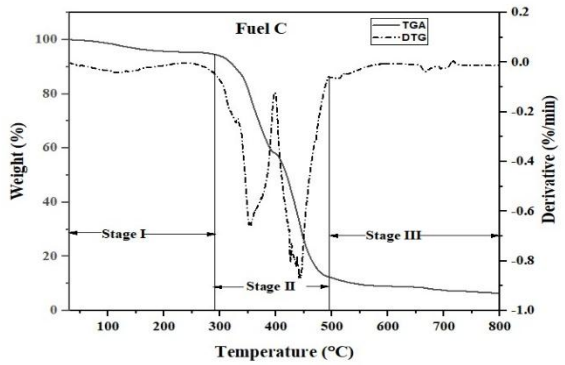

Figure 5. TGA/DTG curves of Combustion Fuel C

temperature range of 30 °C to 900 °C. The results are shown in **Figures 3-5.** As observed from the graphs, three combustions parameters (see **Table 3**) from the TG curves can be used to describe the combustion characteristics, including the ignition temperature Ti, peak temperature Tp, and the burnout temperature T_f. While the ignition temperature represents the temperature at which the samples begin to burn, the peak temperature can be determined from the DTG curve as the temperature at which the maximum rate of mass loss of samples is observed. Also, the burnout temperature corresponds to the temperature at which all the combustibles in the sample have been exhausted (Wnorowska et al., 2021). Besides the combustion parameters, the TG curve can be divided into three main stages to include dehydration stage, active pyrolysis stage, and passive pyrolysis stage. As observed**,** the dehydration stage occurred in the temperature ranges of 30-269.83 °C (A), 30-257.84 °C (B), and 30-250.7 °C (C), respectively. During this stage, the process involved the removal of moisture, extractives, and other light volatile matters. The dehydration stage was further divided into two substages: the first stage involved the release of moisture at around 105°C, followed by the second stage, which involved the release of some light volatiles and gradual degradation of certain pseudo-components such as lignin and hemicellulose. Lignin, a biopolymer, is composed of very strong chemical bonds and, hence, has a wider degradation temperature range. Its degradation, though very slow, has been reported to start at a low temperature of about 160 °C (Virmond et al., 2013), which could span to about 900 °C. Hemicellulose degradation begins beyond 200 °C and could span to around 325 °C (Sikarwar et al., 2016). Hemicellulose is a polymer of simple sugars whose binding bonds can be easily broken down in these low temperature ranges. Also, cellulose, mainly a straight chain polymer of anhydroglucopyranose connected by ether bonds, decomposes between 300 and a bit beyond 400 °C (Zhang & Zhang, 2019). Thus, the active pyrolysis stage occurred between the temperature ranges of 269.83-436.67 °C (A), 257.84-433.65 °C (B), and 250.7-443.03 °C (C), respectively (**Table 2**). A similar trend of mass loss rates was observed for the three combustion fuels. The active pyrolysis stage can also be sub-divided into two stages of hemicellulose and cellulose decomposition as evident by the peaks from the DTG curves. Volatiles are released because of thermal degradation of hemicellulose. Further beyond 325 °C as observed, (there were two major peaks observed for all samples with the sharper peak corresponding to the temperature where the major mass loss occurred), major mass loss occurred with sample C having the highest peak temperature (443.03 °C). It can be argued that through the temperature ranges discussed, there is an overlap between decompositions of the three pseudo-components making up the biomass samples. Moreover, the active pyrolysis stage accounted for the major mass loss of all the samples considered with sample B having the highest release of volatiles, while sample A had the least amount of volatiles**.** These temperature ranges make the biomass samples suitable for thermochemical processes. The thermal

Table 2. Summary of combustion stages, ignition, peak, and burnout temperatures of combustion fuels

Combustion Fuels	Stages (°C)	T_i (°C)	T_p (°C)	T_f (°C)	Mass loss at T_p (%)
A	30 -269.83	269.83	436.66	755.49	69.9
	269.83 - 344.54				
	344.54 - 436.66				
B	30 -257.84	355.54	433.65	751.15	84.75
	257.84 -355.54				
	355.54 - 433.65				
C	30 -250.7	250.7	443.03	772.07	84.48
	250.7 -354.52				
	354.52 - 443.03				

decomposition of the combustion fuels in the current study followed similar trends of thermal decomposition of a typical biomass as found elsewhere (Castells et al., 2021; Emiola-sadiq et al., 2021).

4.2 Determination of Kinetic Parameters of Combustion fuels

The TGA data was used to fit the 16 different kinetic models to determine three kinetic triplets: reaction mechanism, activation energy, and pre-exponential factor. By using the C-R model fitting method, the model with the best calculated $R^2 \geq 0.95$ was chosen as the best model to describe the thermal decomposition of the combustion fuels. As observed from the DTG curves from Section 3.1, two peaks corresponding to temperatures where major mass losses occurred were found. Based on the peaks, TGA data sets for the three biomass samples were divided into three and two sections, respectively, fitted separately to represent two different temperature regions. The first temperature region (30-160 °C) was omitted from the analysis as was explained in Section 3.1 (the stage where moisture and other light volatiles were lost). These temperature regions corresponded to different conversion regions for the samples. The types of models chosen were power models, nucleation models, diffusion models, reaction order models, and geometrical contraction models. The plots of the different kinetic models in **Figure 6a-c** are suggestive of different mechanisms of thermal decomposition characterizing distinct temperature regions despite thermal similarities observed for the samples. As seen in **Figure 6a,** each region (I and II) can be assumed to have a distinct kinetic model describing the decomposition.

Table 3. Results of the kinetic parameters of the three combustion fuels

A	
Region/Kinetic Parameters	**Region/Kinetic Parameters**
$0 < \theta < 0.4\ (160 - 345.4^{O}C)$	$0.4 < \theta < 0.99\ (Above\ 345.4^{O}C)$
Average $E_\theta = 101.95\ kJ/mol$	$E_\theta = 135.00\ kJ/mol$
Average $k_o = 1.57 \times 10^{14} min^{-1}$	$k_o = 5.29 \times 10^{14} min^{-1}$
$g(\theta) = F0/D2/D4/D1/D3 -$ Zero/Diffusion Models	$g(\theta) = D4 -$ Diffusion model
$Average\ R^2 = 0.9541$	$R^2 = 0.963$
B	
$0 < \theta < 0.5\ (160 - 358.20^{O}C)$	$0.5 < \theta < 0.99\ (Above 358.20^{O}C)$
Average $E_\theta = 19.15\ kJ/mol$	$E_\theta = 40.21\ kJ/mol$
Average $k_o = 2.39 \times 10^{5} min^{-1}$	$k_o = 3.88 \times 10^{7} min^{-1}$
$g(\theta) = P2/AE2 -$ Power law/Avrami − Erofeev Models	$g(\theta) = AE2 -$ Avrami − Erofeev Model
$Average\ R^2 = 0.9528$	$R^2 = 0.9821$
C	
$0 < \theta < 0.65\ (160 - 343.94^{O}C)$	$0.65 < \theta < 0.99\ (Above 343.94^{O}C)$
$E_\theta = 19.67\ kJ/mol$	$E_\theta = 287.03\ kJ/mol$
$k_o = 2.92 \times 10^{5} min^{-1}$	$k_o = 3.5 \times 10^{28} min^{-1}$
$g(\theta) = P4 -$ Power law model	$g(\theta) = D2 -$ Diffusion Model
$R^2 = 0.9515$	$R^2 = 0.9996$

130

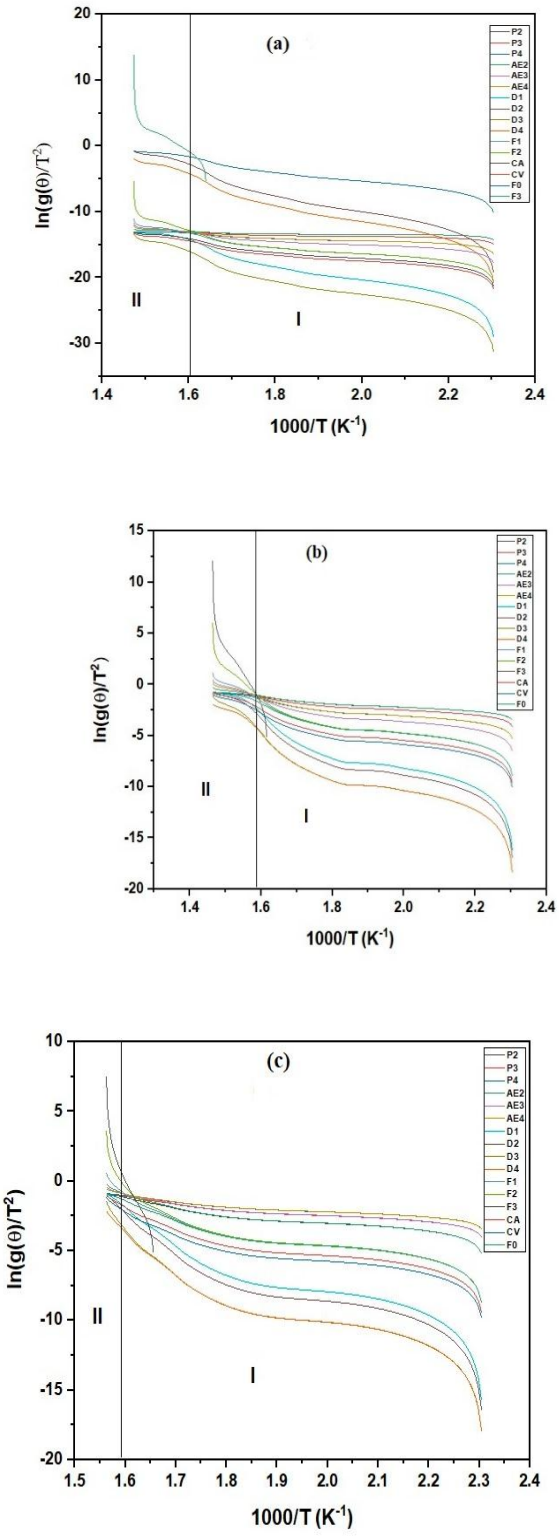

Figure 6. Integral plot of different theoretical kinetic models using the C-R model-fitting method: (a) combustion fuel A; (b) combustion fuel B; (c) combustion fuel C

In the conversion region of $0 < \theta < 0.4$ (stage I), the experimental plot fitted best with the zero-order (F0) model (R^2 =0.9599) for combustion fuel A. Diffusion models (D2/D4/D1/D3) have R^2 values > 0.95 in this region. The zero-order model is a nucleation-based model which assumes instabilities in a bulk solid's local energies due to several factors such as presence of impurities, point defects, cracks, and so on. The fluctuations in the local energies may then result in gradual reaction (nucleation) at the site and nucleation site at low activation energy. The zero-order model could mean a diffusion-controlled movement of the product nucleation mechanism which explains why diffusion models (D2/D4/D1/D3) were a good fit in this region (Rony et al., 2019). The region above 0.4 (stage II) conversion values coincide with Ginstling–Brounshtein (D4) model with $R^2 = 0.963$ (**Table 3**).

The plots for combustion fuel B are presented in **Figure 6b.** A similar trend was observed for B, as observed for A. However, unlike A, power law (P2 with $R^2 = 0.9551$) was the model with the best fit with Avrami-Erofeev models (AE2) also having R^2 value > 0.95 in the region below 0.5 conversion values. Both models are nucleation models, with the former assuming constant nuclei growth and the latter assuming a restraint in nuclei growth. Furthermore, the lowest order magnitude of the Avrami-Erofeev models (AE2) with R^2 value of 0.9821 fitted the decomposition of B at conversion values > 0.5. Similarly, **Figure 6c** shows the integral plots for the combustion fuel C for the two regions. Here, the power law model (P4) coincides with the decomposition mechanism of the region with conversion values $\theta <$ 0.65. The decomposition mechanism in this region is similar to what was reported for willow sawdust in a previous study (Emiola-sadiq et al., 2021). At conversion values > 0.65, the diffusion controlled (D2) model was best fit for the biomass decomposition with R^2 value of 0.9996. These results ascertained the complexity/multi-reaction mechanism for the decomposition of the biomass samples. The complex mechanism of decomposition may be due to the overlapping regions of decomposition of the three pseudo-components (lignin, hemicellulose, and cellulose) with the temperature decomposition range of one spanning into another, hence accounting for the complexity of reaction mechanism.

Table 3 presents the estimated values of the activation energies E_θ and pre-exponential factors k_o for the three biomass samples in the two regions considered in the current study. As discussed earlier, kinetic

parameters were estimated for the regions differently. The estimated activation energies for Region I for the three biomass samples are 101.95, 19.15, and 19.67 kJ/mol, respectively. At higher conversion values (region II), the values ranged from 135.00, 40.21, and 287.03 kJ/mol for combustion fuels A, B, and C, respectively. By juxtaposing the two regions, as expected, the activation energies were observed to be lower in region I when compared to II. Region I is dominated by hemicellulose decomposition, which requires less energy to break the intermolecular bonds compared to cellulose, a more complex biopolymer. Meanwhile, the kinetics of lignin decomposition is slow and spans over a wider temperature range and, hence, may require greater activation energy. This may also account for the rise in the activation energies in Region II due to a shift to higher temperatures. The trend observed for activation energies in Region II indicates that activation energy increases with increasing conversion values. The C-R method has been successfully used to determine the kinetic triplets of the three biomasses considered. Mishra & Mohanty (2021) evaluated the kinetic parameters of three varieties of lignocellulosic biomass using the C-R method. The decomposition kinetics of *Parthenium hysterophorus* using the C-R method have also been reported elsewhere (Dhaundiyal et al., 2018).

4.3 Effect of Combustion Fuel Types on Temperature Profile and Biochar Yield

The temperature profiles were monitored for the six batch carbonization processes. Each fuel type was used to conduct two different carbonization experiments to observe its effects on biochar yields from R1 and R2. As reported in a previous study (Adeniyi et al., 2020), temperature measurements are taken from four different points on the reactor. Three of those points are to monitor the downward progression of the combustion zone within the heating space of the reactor, while the fourth point is a better representation of the temperature condition within the reactor chamber. In the current study, the reactor temperature profiles for the six carbonization experiments are displayed in **Figures 7-9**. Temperature measurements were taken at 10-minute intervals to observe the progression of the carbonization process.

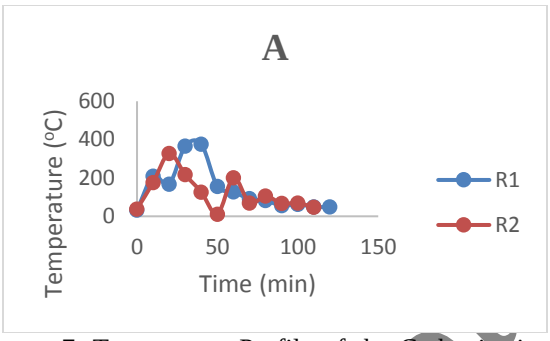

Figure 7. Temperature Profile of the Carbonization process using Fuel A

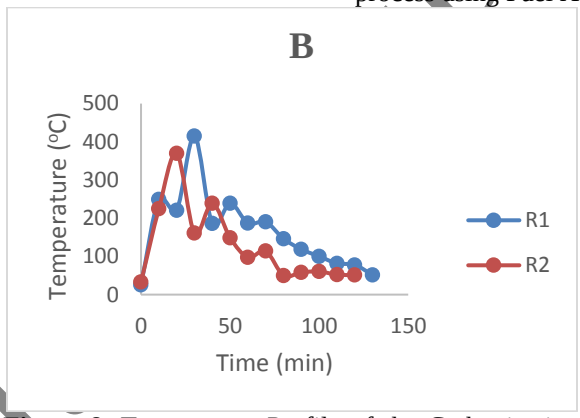

Figure 8. Temperature Profile of the Carbonization process using Fuel B

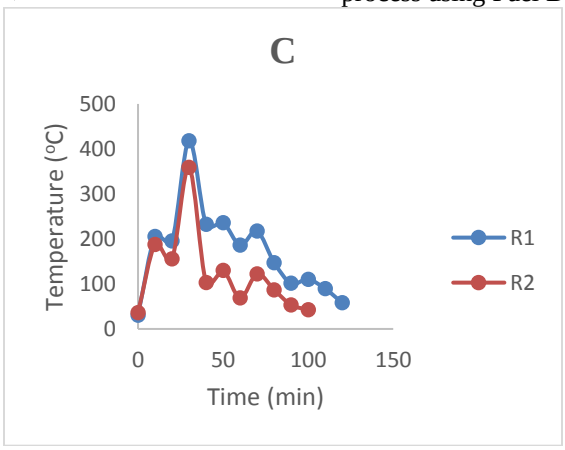

Figure 9. Temperature Profile of the Carbonization process using Fuel C

Table 4. Summary of Biochar yields and Peak Carbonization Temperatures

	R1		R2	
Fuel Type	**Yield (%)**	**Peak Temperature (°C)**	**Yield (%)**	**Peak Temperature (°C)**
A	64.6	376.2	28.4	327.4

130
c

B	37.8	415.2	24.5	370
C	45.2	418.3	24.8	358.8

A critical study of **Figures 7-9** indicates the temperature profiles to follow the same pattern as what was obtained from previous studies reviewed earlier in Section 1. The temperature rose gradually (though an irregular rise) until it reached a peak temperature before a persistent drop in temperature was observed. Different peak temperatures ranging from 376.2-415.2 ^{o}C for R1 and 327.4-370 ^{o}C for R2 (see **Table 4**) were recorded for the six batch experiments. For the three fuel types, peak temperatures for R1 carbonization were consistently higher than those for R2. Although combustion fuels are necessary to provide the heat to drive an early endothermic reaction within the carbonization chamber, at some point, devolatilization will be accompanied by loss of heat, hence a rise in the temperature. Therefore, thermochemical conversion of R1(corn husk) in the carbonization chamber is more exothermic than that of R2 (corn cob), thus accounting for the higher peak temperatures for R1 in the three cases. This observation is consistent with findings from a previous study (Intani et al., 2016).The effects of varying peak temperatures on the yields of biochar from the two biomass sources are also displayed in **Table 4.** A negative correlation was found between biochar yields and increasing peak temperatures. The trend was more observable with R2 as biochar yield decreased with increasing temperature. Biochar yield from R1 using combustion fuel A was 64.6 % at 376.2 ^{o}C. A further reduction was observed in biochar yield from R1 using combustion fuel B at a peak temperature of 415.2 ^{o}C (biochar yield was 37.8 %). However, biochar yield was higher (45.2 %) in the third case with combustion fuel C even though the process peaked at a higher temperature (418.3 ^{o}C) deviating from the trend observed with R2. The R1 sample used in the third experiment may have had more moisture content and impurities, hence the deviation from the trend. A similar trend of the negative correlation between biochar yield and increasing temperature for both slow and fast pyrolyses of walnut (Yuan et al., 2020) was reported earlier. However, at above 600 ^{o}C, the trend was reported insignificant, indicating that the decreasing trend observed in yield of biochar occurred at temperatures below 600 ^{o}C. Other studies in the literature have also made similar observations, including studies by authors (Intani et al., 2018; Masek et al., 2013) . **Table 5** presents a comparison between the key findings in this study and those from previous works from the same process. Despite similar effects of combustion fuels on the yields of biochars produced from the two biomass sources considered in the current study, combustion fuel A can be considered the best amongst the three fuels in terms of high biochar yield.

Table 5. Comparison of the current study with previous works using the same retort system.

4.5 Comparison between Peak Temperatures of Combustion Fuels from TGA and Carbonization Experiments

The temperature profile of a typical retort heated carbonization reactor was discussed in the preceding section (see **Figure 2**). A critical evaluation of thermographs obtained for both TGA (**Figures 3-5**) and carbonization experiments (**Figures 7-9**) showed that combustion fuels underwent similar decomposition stages. From the TGA, with increasing temperature, the combustion fuels undergo loss in weight gradually until it reaches a temperature (peak temperature Tp) where maximum mass loss was observed. The maximum energy (thermal capacity) possessed by combustion fuel(s) would be released at this point. Similarly, the temperature profiles from the carbonization experiments exhibited a gradual rise in temperature until a peak temperature was reached (referred to as peak carbonization temperature PCT).

Biomass	Combustion Fuel Used	PCT (ºC)	TGA Tp for Combustion Fuel (ºC)	Biochar Yield (%)	Estimated E_θ for Combustion Fuel (KJ/mol)	Reference
Plantain Fibers	Dry bamboo + African balsam	220		6.98		(Adeniyi et al., 2019a)
Elephant grass	Dry bamboo + African balsam	300		14.29		(Adeniyi et al., 2019b)
Elephant grass	Dry bamboo + African balsam	371		27.3		(Adeniyi et al., 2020)
Elephant grass + LDPE	Dry bamboo + African balsam	382		13.8		(Adeniyi et al., 2020)
Sugarcane bagasse	Daniella Olivera	349		16.67		(Adeniyi et al., 2020)
Sugarcane bagasse +LDPE	Daniella Olivera	250		45.46		(Adeniyi et al., 2020)
Dry almond leaves + LDPE	Daniella Olivera	494		71.43		(Ighalo et al., 2021)
Dry almond leaves	Daniella Olivera	362		28.57		(Ighalo et al., 2021)
Corn Husk	A	376.2	436.66	64.6	101.95 - 135.00	Current Study
Corn Husk	B	415.2	433.65	37.8	19.15 - 40.21	Current Study
Corn Husk	C	418.3	443.03	45.2	19.67- 287.03	Current Study
Corn cob	A	327.4	436.66	28.4	101.95 - 135.00	Current Study
Corn Cob	B	370	433.65	24.5	19.15 - 40.21	Current Study
Corn cob	C	358.8	443.03	24.8	19.67- 287.03	Current Study

Table 6. Peak Temperatures from TGA and Carbonization Experiments

Combustion	TGA Peak	R1 PCT	R2 PCT

130
o

Fuel	Temperature Tp (ºC)	(ºC)	(ºC)
A	436.66	376.2	327.4
B	433.65	415.2	370
C	443.03	418.3	358.8

During this temperature rise, combustion fuels underwent thermal decomposition like that obtained from the TGA. Hence, upon comparing the peak temperatures obtained from TGA and carbonization experiments, we found that the Tps were higher than the PCTs (**Table 6**) obtained for both R1 and R2. The implication is that thermal efficiencies of combustion fuels were not attained in the reactor due to loss of heat because of devolatilization of volatile gases through the exhaust pipe of the reactor, conduction, and convection. Factors that may be responsible for thermal inefficiency include environmental factor (rate of airflow into the reactor to support the controlled combustion may be largely responsible for the self-regulating nature of the process) and reactor material type. The reactor used in the current study was fabricated from stainless steel, which is a good conductor of heat. It may be interesting to further explore how to optimize the thermal efficiencies of combustion fuels in the reactor by introducing a lagging support, improving the design of the reactor exhaust, and considering other material types for reactor design.

Biochar Characterization 4.6

The morphologies of the six biochar samples were studied using the scanning electron microscope (SEM) with the acceleration voltage set at 15 kV and the micrographs obtained at different magnifications. The micrographs are displayed in **Figure 10(a-f)** at 500x magnification and estimated particle sizes at 100 μm.

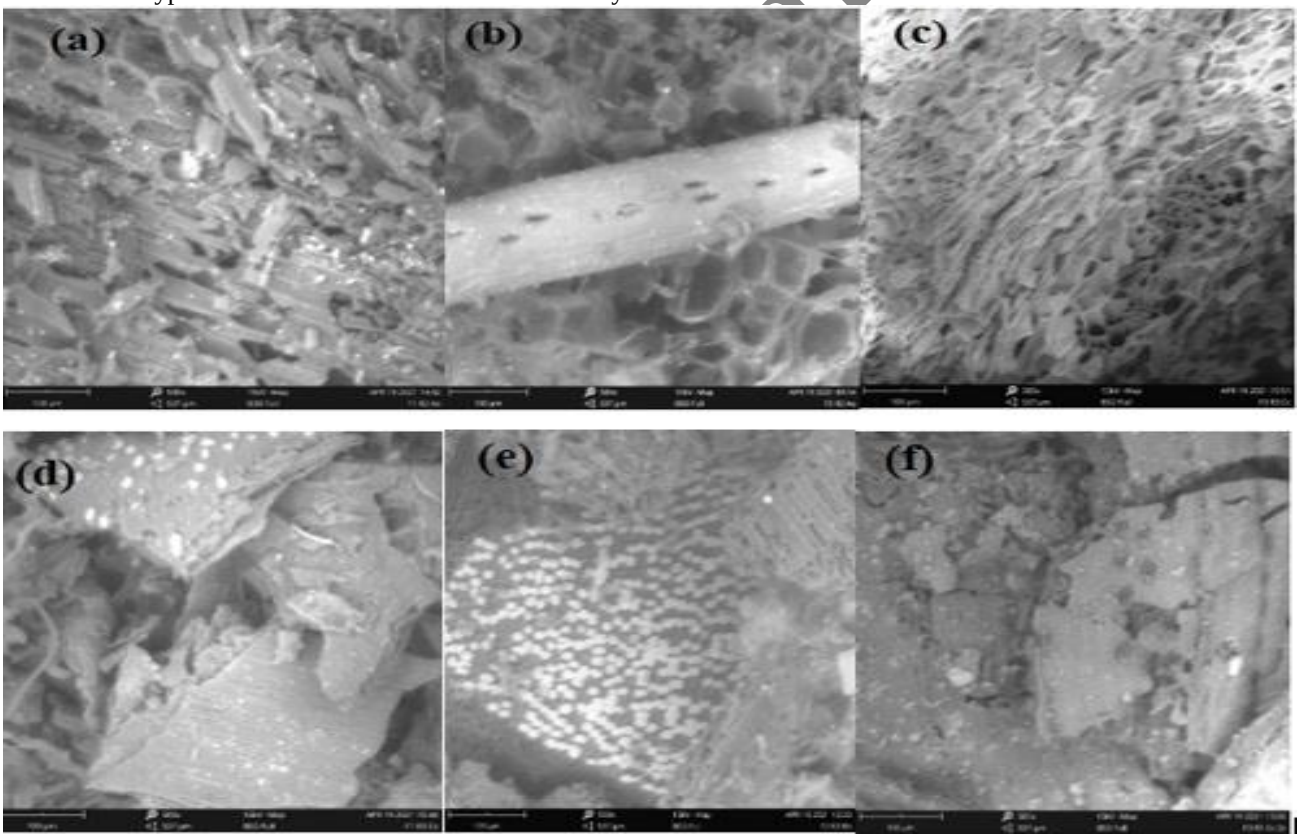

Figure 10. Micrographs of biochar samples (a)-(c) biochars from R1 with combustion fuels and (d)-(f) biochars from R2 with combustion fuels.

As can be seen in **Figure 10a-c**, the surfaces of the R1 biochar samples with different combustion fuels appeared to have similar patterns of surface formations. A homogeneous, porous outlook with visible formations of craters (similar to that of neem leaves) (Ighalo & Adeniyi, 2020) arranged in a

stepwise manner was observed. Furthermore, R2 biochar samples (**Figure 10d-f**) were observed to have harder surfaces with irregular patterns characterized with small white patches arranged in a regular sequence (more visible on **d** and **e**). However, the white patches were found scattered on biochar sample **f**. The white patches have been suggested to be oxides of either potassium or silicon (Adeniyi et al., 2020). This observation was corroborated with the EDS analysis of the samples.

Table 7. Elemental Composition of R1 with Combustion Fuels

	A	B	C
Element	**Atomic Concentration (%)**	**Atomic Concentration (%)**	**Atomic Concentration (%)**
Carbon	68.23	61.55	45.67
Potassium	18.1	8.71	18.32
Chlorine	5.41	1.65	4.28
Nitrogen	3.65	1.47	2.25
Phosphorus	1.31	0.69	0.96
Oxygen	1.56	2.02	2.93
Silicon	0.57	19.35	17.91
Aluminium	0.49	0.73	0.87
Magnesium	0.46	0.15	0.55
Sulfur	0.33	0.4	1.66
Calcium	0.15	2.65	3.54
Sodium	0.24	0.22	0.29
Titanium	0	0	0
Iron	0	0	0.77

Table 8. Elemental Composition of R2 with Combustion Fuels

	A	B	C
Element	**Atomic Concentration (%)**	**Atomic Concentration (%)**	**Atomic Concentration (%)**
Carbon	77.13	76.42	82.26
Potassium	10.06	7.91	6.02
Chlorine	1.42	1.26	0.83
Nitrogen	0.86	0.5	3.14
Phosphorus	1.26	0.68	0.81
Oxygen	2.33	1.65	2.93
Silicon	3.82	9.41	1.1
Aluminium	0.79	0.71	1.55
Magnesium	0.6	0.21	0.5
Sulfur	0.77	0.48	0.54
Calcium	0.4	0.53	0

131
0

Sodium	0.56	0.23	0.32
Titanium	0	0	0
Iron	0	0	0

The elemental compositions of the biochar samples were recorded using the EDS analysis (see **Tables 7&8).** As expected, carbon had the highest composition of elements present in the samples with compositions ranging from 45.67- 68.23 % for R1 and 77.13-82.26 % for R2. Interestingly, all the samples contained N, P, and K in substantial amounts. These are important elements providing nutrients for plant growth in soils (Naeem et al., 2017). The corresponding EDS spectra of the focused area of the SEM images of the samples are displayed in **Figures 11-16.** Contrasting peak intensities were observed for all the samples showing elevated peaks of K and Si. Si is another element that has been studied extensively recently because of its potential to reduce toxic effects heavy metals can have on crops and improving soil nutrients (Karam et al., 2022; Rizwan et al., 2019) .

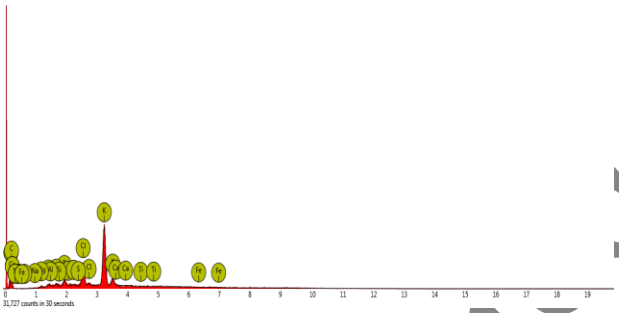

Figure 11. EDS Spectrum of R1 with Combustion Fuel A

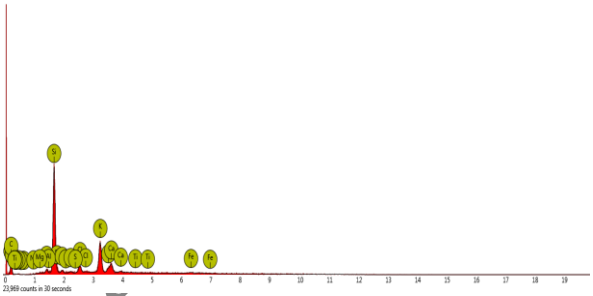

Figure 12. EDS Spectrum of R1 with Combustion Fuel B

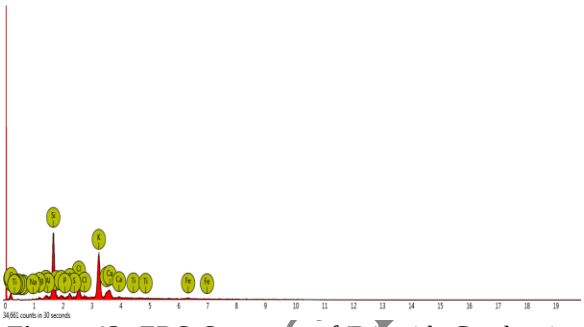

Figure 13. EDS Spectrum of R1 with Combustion Fuel C

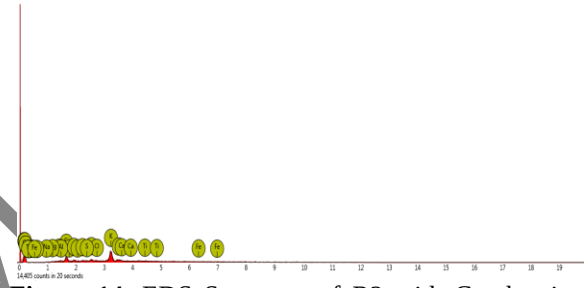

Figure 14. EDS Spectrum of R2 with Combustion Fuel A

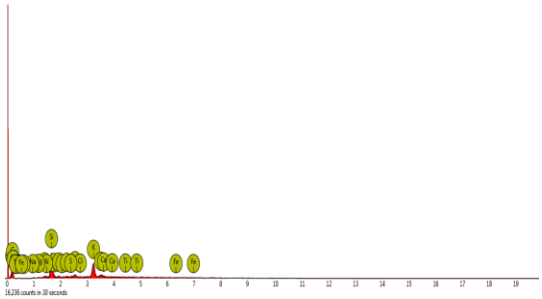

Figure 15. EDS Spectrum of R2 with Combustion Fuel B

Figure 16. EDS Spectrum of R2 with Combustion Fuel C

In addition, the effects of different combustion fuels on the functional groups present in biochar samples were also studied using the FTIR, as shown in **Figures 17-18.** Similar spectra were observed for the R1 samples. However, the peaks were more distinct in the biochar sample with combustion fuel A. The intensity of some of the peaks were observed to have faded away for the samples with combustion fuels B and C (more apparent with B, see **Figure 17**). This is because at higher temperatures, most of the functional groups are lost, explaining the observation with samples obtained with combustion fuels B and C. The loss of functional groups with increasing temperature has been observed in a recent study (Janu et al., 2021). The authors observed that increasing the pyrolysis temperature to 750 °C led to the mentioned loss at all wavenumbers for conifer wood.

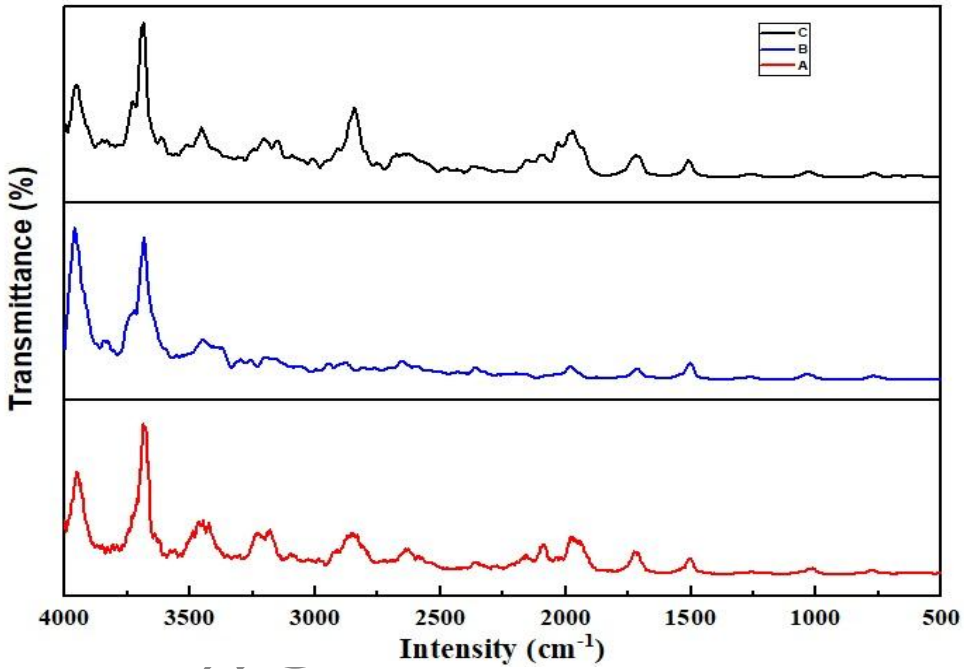

Figure 16. FTIR Spectra of R1 with Combustion Fuels

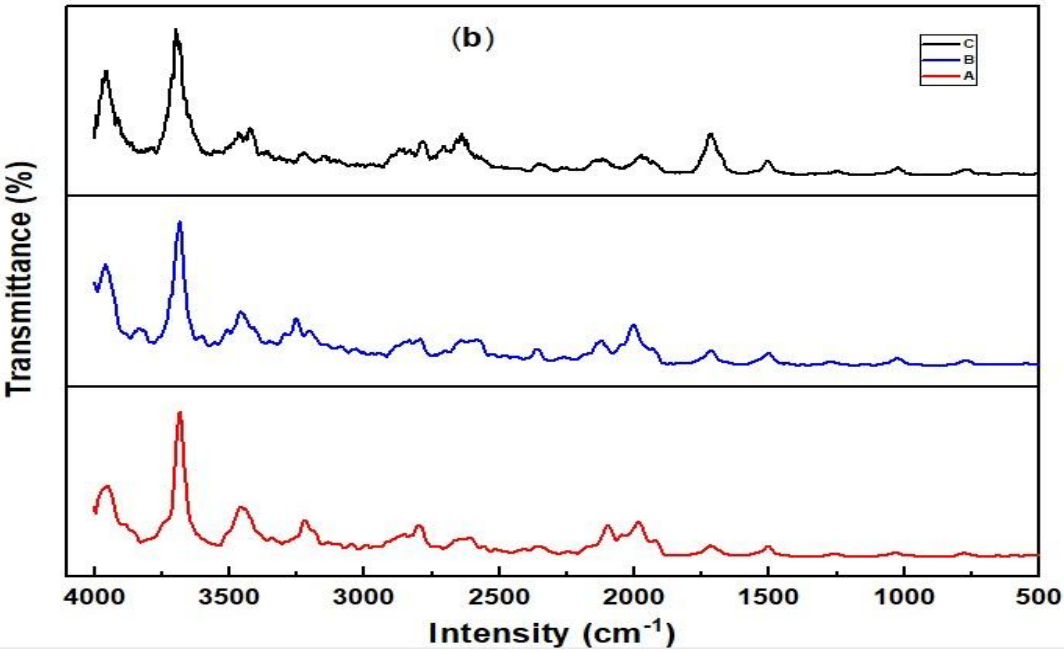

131
2

Figure 17. FTIR Spectra of R2 with Combustion Fuels

Conversely, for R2 biochar samples, the spectra were observed to be similar for all combustion fuels, with only a major peak in the region of 2000-1500 cm^{-1} being more apparent for the sample with combustion fuel C. Major differences may not have occurred due to the similar peak carbonization temperatures (PCT) recorded for the samples (PCT ranged between 327.4-370 ^oC). In the work of Ma et al. (2017), they observed that the intensity of peaks assigned to functional groups remained distinct and unaffected in the temperature range of 250-350 ^oC (an explanation for the observation with R2 biochar samples). They further opined that at above 450 ^oC, gradual loss of functional groups attributed to cracking of more complex structures in the biomass under intense temperature would begin to set in. Their observations further corroborated the observation for R1 biochar samples. The peaks observed for R1 (3954.35 cm^{-1} and 3645.78 cm^{-1}) and R2 (3652.92 cm^{-1}) were attributed to the hydroxyl -OH stretching vibration due to cellulose and hemicellulose dehydration found in most biomass sources (Amoloye et al., 2022; Ighalo et al., 2020; Nandiyanto et al., 2019). The regions of 3202.91 cm^{-1} and 3247.30 cm^{-1} (R1) were assigned to aromatic C-H stretching and the peak observed at 3498.63 cm^{-1} (R2) could be attributed to the medium non-bonded (-OH) hydroxyl group (Adeniyi et al., 2022). Further, the aliphatic C-H stretching was assigned to the peaks found in the regions 2855.76 cm^{-1} (R1) and 2805.76 cm^{-1} (R2) (Kang et al., 2012). Isothiocyanate (-NCS) groups could be attributed to peaks at 2047 cm^{-1} (R1) and those at 2137.18 cm^{-1} and 1995.78 cm^{-1} (R2) (Nandiyanto et al., 2019) due to the presence of N and S, as confirmed by the EDS analysis. Another peak found at 3141.48 cm^{-1} (R2) has been assigned to the aromatic C-H stretching (Adeniyi et al., 2022) while the one found at 1492.88 (R1) suggests the presence of aromatic nitro-compounds (Nandiyanto et al., 2019). Overall, it was found that all the samples contained hydroxyl (-OH) groups, which make the biochars hydrophilic (Ghani et al., 2013) . This characteristic makes them potentially useful for water-related applications and as soil amendments. The effects of three forest biomasses used as combustion fuels for carbonization of R1 and R2 on the qualities of biochars produced were similar.

5. CONCLUSIONS

In this study, the thermal properties, and kinetic parameters of three different biomass sources (*acacia auriculiformis* (A), *terminalia randii* (B), and *delonix regia* (C)) sources as combustion fuels were investigated. The effects of these biomass sources on the yields and qualities of biochars produced from the retort carbonization of corn husk (R1) and cob (R2) were successfully examined. The following conclusions were drawn:

1. Combustion fuels have similar thermal properties with peak temperatures of 436.66 ^oC (A), 433.65 ^oC (B), and 443.03^oC(C).
2. Estimated E_θ values ranged between 101.95-135 kJ/mol for combustion fuel A, 19.15-40.21 kJ/mol (B), and 19.67-287.03kJ/mol (C).
3. Negative correlation was found between biochar yields and increasing carbonization temperatures.
4. Carbon-rich products were produced with carbon contents ranging from 45.67-68.23% for R1 and 77.13-82.26% for R2.
5. Combustion fuels were found to have similar effects on the functional groups present in the biochar samples.

6. ACKNOWLEDGEMENT

The contributions of Mutiat Oniye and Ogunniyi Samuel, postgraduate students at the Department of Chemical Engineering, University of Ilorin, during the experimental runs are highly appreciated.

NOMENCLATURE

A	*Acacia auriculiformis*
B	*Terminalia randii*
C	*Delonix regia*
$k(T)$	Constant dependent on temperature
$f(\theta)$	Function describing the path or mechanism of the reaction.
R	Universal gas constant (J/K.mol)
T	Reaction temperature (^oC)
R1	Corn Husk
R2	Corn Cob
M_1	mass of the feed chamber + feed (g)
M_2	mass of feed chamber (g)
M_3	mass of the feed chamber + product (g)
Ti	Ignition temperature
Tp	Peak temperature
T_f	Burnout temperature

Greek letters

θ	Extent of conversion
ε_o	Initial mass of sample
ε_t	Mass of sample at any time t
ε_f	Final mass of sample
k_o	pre-exponential factor (s^{-1})
E_θ	Activation energy (kJ/mol)
$g(\theta)$	Integral form of the conversion function
β	Heating rate (^oC/min)
$p(x)$	Integral form of the temperature term

REFERENCES

Adeniyi, A. G., Ighalo, J. O., Onifade, D. V, and Popoola, A. O., "Production of Hybrid Biochar by Retort-Heating of Elephant Grass (Pennisetum Purpureum) and Low Density Polyethylene (LDPE) for Waste Management and Product Development", ***Journal of Materials and Environmental Science,*** Vol. *2508*, *No.* 12, (2020), 1940–1952. (https://doi.org/10.1080/17597269.2019.1613751)

Adeniyi, A. G., Abdulkareem, S. A., Adeyanju, C. A., and Ighalo, J. O.,"Recycling of Delonix regia Pods Biochar and Aluminium Filings in the Development of Thermally Conducting Hybrid Polystyrene Composites", ***Journal of Polymers and the Environment***, (2022). https://doi.org/10.1007/s10924-022-02413-5

Adeniyi, A. G., Abdulkareem, S. A., Ighalo, J. O., Onifade, D. V., and Sanusi, K. S. "Thermochemical Co-conversion of Sugarcane Bagasse-LDPE Hybrid waste into Biochar", ***Arabian Journal for Science and Engineering***, (2020).(http://dx.doi.org/10.1007/s13369-020-05119-9)

Adeniyi, A. G., Ighalo, J. O., and Onifade, D. V.,"Production of Bio-Char from Plantain (musa Paradisiaca) Fibers Using an Updraft Biomass Gasifier with Retort Heating", ***Combustion Science and Technology***, (2019a), 1–15. https://doi.org/10.1080/00102202.2019.1650269

Adeniyi, A. G., Ighalo, J. O., and Onifade, D. V., "Production of biochar from elephant grass (Pernisetum purpureum) using an updraft biomass gasifier with retort heating", ***Biofuels***, (2019b),1–8. (https://doi.org/10.1080/17597269.2019.1613751)

Amoloye, M. A., Abdulkareem, S. A., and Adeniyi, A. G., "Comparative Study of Biochars from the Retort Co-Carbonization of Corn Cob and Polyethylene Wastes", ***Malaysian Journal of Catalysis***, No. *7*, (2023), 6–12. (http://dx.doi.org/10.11113/mjcat.v7n1.168)

Amoloye, Mubarak Adewale, AbdulKareem, S. A., & Adeniyi, A. G. (2022). Production and Characterization of Biochar and Hybrid Produced from the Co-carbonization of Corn Husk and Low-Density Polyethylene Wastes. In *Bioenergy and Biochemical Processing Technologies* (pp. 13–25). (https://doi.org/10.1007/978-3-030-96721-5_2).

Castells, B., Amez, I., Medic, L., Fernandez-anez, N., and Garcia-torrent, J., "Study of lignocellulosic biomass ignition properties estimation from thermogravimetric analysis", ***Journal of Loss Prevention in the Process Industries***, (2021). (https://doi.org/10.1016/j.jlp.2021.104425)

Coats, A. W., and Redfern, J. P., "Kinetic Parameters from Thermogravimetric Data", ***Nature***, Vol. *201*, (1964), 68–69. (https://doi.org/10.1038/201068a0)

Dhaundiyal, A., Singh, S. B., Hanon, M. M., and Rawat, R., "Determination of Kinetic Parameters for the Thermal Decomposition of Parthenium hysterophorus", ***Environmental and Climate Technologies***, Vol. *22*, (2018), 5–21. (https://doi.org/10.1515/rtuect-2018-0001)

Emiola-sadiq, T., Zhang, L., and Dalai, A. K., "Thermal and Kinetic Studies on Biomass Degradation via Thermogravimetric Analysis : A Combination of Model-Fitting and Model-Free Approach", ***ACS Omega***, Vol. *6*, (2021), 22233–22247. (https://doi.org/10.1021/acsomega.1c02937)

Ghani, W. A. W. A. K., Mohd, A., da Silva, G., Bachmann, R. T., Taufiq-yap, Y. H., Rashid, U., and Al-Muhtaseb, A. H.,"Biochar production from waste rubber-wood-sawdust and its potential use in C sequestration : Chemical and physical characterization", ***Industrial Crops & Products***, Vol. *44*, (2013), 18–24. (https://doi.org/10.1016/j.indcrop.2012.10.017)

Hildago-oporto, P., Navia, R., Hunter, R., Coronado, G., and Gonzalez, M. E., "Synthesis of carbon nanotubes using biochar as precursor material under microwave irradiation", ***Journal of Environmental Management***, Vol. 244, (2019), 83–91. (https://doi.org/10.1016/j.jenvman.2019.03.082).

Ighalo, J. O., Adeniyi, A. G., Omodele, A. A. E., Lois, T., and Arowoyele, T., "Competitive adsorption of Pb (II), Cu (II), Fe (II) and Zn (II) from aqueous media using biochar from oil palm (Elaeis guineensis) fibers : a kinetic and equilibrium study fibers : a kinetic and equilibrium study", ***Indian Chemical Engineer***, (2020), 1–11. (https://doi.org/10.1080/00194506.2020.1787870)

Ighalo, J. O., and Adeniyi, G. A., "A mini ‐ review of the morphological properties of biosorbents derived from plant leaves", ***SN Applied Sciences***, (2020). (https://doi.org/10.1007/s42452-020-2335-x)

Ighalo, J. O., Onifade, D. V., and Adeniyi, A. G., "Retort-heating carbonisation of almond (Terminalia catappa) leaves and LDPE waste for biochar production: evaluation of product quality", ***International Journal of Sustainable Engineering***, (2021), 1–9. (https://doi.org/10.1080/19397038.2021.1886371)

Intani, K., Latif, S., Cao, Z., and Müller, J.,"Characterisation of biochar from maize residues produced in a self-purging pyrolysis reactor", ***Bioresource Technology***, (2018). (https://doi.org/10.1016/j.biortech.2018.05.103)

Intani, K., Latif, S., Kabir, A. K. M. R., and Müller, J., "Effect of self-purging pyrolysis on yield of biochar from maize cobs , husks and leaves", ***Bioresource Technology***, Vol. *218*, (2016), 541–551.(https://doi.org/10.1016/j.biortech.2016.06.114)

Janu, R., Mrlik, V., Ribitsch, D., Hofman, J., Sedlacek, P., Bielska, L., and Soja, G., "Biochar surface functional groups as affected by biomass feedstock , biochar composition and pyrolysis temperature", ***Carbon Resources Conversion***,Vol. 4, (2021), 36–46. (https://doi.org/10.1016/j.crcon.2021.01.003)

Kajina, W., and Rousset, P.,"Coupled effect of feedstock and pyrolysis temperature on biochar as soil amendment", (2018). (https://agritrop.cirad.fr/590896/1/indonesia%20IC%20star%202018.pdf)

Kang, S., Li, X., Fan, J., and Chang, J., "Characterization of Hydrochars Produced by Hydrothermal Carbonization of Lignin , Cellulose , D -Xylose , and Wood Meal", ***Industrial & Engineering Chemistry Research***, Vol. *51*, (2012), 9023–9031.(http://dx.doi.org/10.1021/ie300565d)

Karam, D. S., Nagabovanalli, P., Rajoo, K. S., Fauziah, I. C., Abdu, A., Rosli, Z., Muharam, F. M., and Zulperi, D., "An overview on the preparation of rice husk biochar , factors affecting its properties , and its agriculture application", ***Journal of the Saudi Society of Agricultural Sciences***, Vol. *21*, *No.* 3, (2022), 149–159. (https://doi.org/10.1016/j.jssas.2021.07.005)

Leeq, J. W., Kidder, M., Evans, B. R., Paik, S., Buchanan III, A. C., Garten, C. T., and Brown, R. C., "Characterization of Biochars Produced from Cornstovers for Soil Amendment Characterization of Biochars Produced from Cornstovers for Soil", ***Environmental Science and Technology***, Vol. *44*, (2010), 7970–7974. .(https://dr.lib.iastate.edu/handle/20.500.12876/54997)

Liu, L., Huang, Y., Zhang, S., Gong, Y., Su, Y., Cao, J., and Hu, H., "Adsorption characteristics and mechanism of Pb (II) by agricultural waste-derived biochars produced from a pilot-scale pyrolysis system", ***Waste Management***, Vol. *100*, (2019),287–295. (https://doi.org/10.1016/j.wasman.2019.08.021)

Ma, Z., Yang, Y., Ma, Q., Zhou, H., Luo, X., Liu, X., & Wang, S., "Evolution of the chemical composition, functional group, pore structure and crystallographic structure of bio-char from palm kernel shell pyrolysis under different temperatures", ***Journal of Analytical and Applied Pyrolysis***, (2017). (https://doi.org/10.1016/j.jaap.2017.07.015)

Masek, O., Brownsort, P., Cross, A., and Sohi, S., "Influence of production conditions on the yield and environmental stability of biochar", ***Fuel***, Vol. 103, (2013), 151–155. (https://doi.org/10.1016/j.fuel.2011.08.044)

Matali, S., Abd Rahman, N., Idris, S. S., and Yaacob, N., "Dynamic Model-Free and Model-Fitting Kinetic Analysis during Torrefaction of Oil Palm Frond Pellets", ***Bulletin of Chemical Reaction Engineering & Catalysis***, Vol. 15, No. 1, (2020), 253–263. (https://doi.org/10.9767/bcrec.15.1.6985.253-263)

Mishra, R. K., and Mohanty, K.,"Kinetic analysis and pyrolysis behavior of low-value waste lignocellulosic biomass for its bioenergy potential using thermogravimetric analyzer", ***Materials Science for Energy Technologies***, Vol. 4, (2021), 136–147. (https://doi.org/10.1016/j.mset.2021.03.003)

Naeem, M. A., Khalid, M., Aon, M., Abass, G., Amjad, M., Murtaza, B., Khan, W. U. D., and Ahmad, N.,"Combined Application of Biochar with Compost and Fertilizer Improves Soil Properties and Grain Yield of Maize", ***Journal of Plant Nutrition***, (2017), 1532–4087. (https://doi.org/10.1080/01904167.2017.1381734)

Nandiyanto, A. D. B., Oktiani, R., and Ragadhita, R.,"How to Read and Interpret FTIR Spectroscope of Organic Material", ***Indonesian Journal of Science & Technology***, Vol. 4,No.1, (2019), 97–118. (http://dx.doi.org/10.17509/ijost.v4i1.xxxx)

Panwar, N. L., Pawar, A., and Salvi, B. L., "Comprehensive review on production and utilization of biochar", ***SN Applied Sciences***, Vol. 1, No. 2, (2019). (https://doi.org/10.1007/s42452-019-0172-6)

Rizwan, M., Rehman, M. Z. ur, Ali, S., Abbas, T., Maqbool, A., and Bashir, A., "Biochar Is a Potential Source of Silicon Fertilizer : An Overview", ***Biochar from Biomass and Waste***, (2019), 225–238.(https://doi.org/10.1016/B978-0-12-811729-3.00012-1)

Rony, H. A., Kong, L., Lu, W., Dejam, M., Adidharma, H., Gasem, A. M. K., Zheng, Y., Norton, U., and Fan, M.,"Kinetics , thermodynamics , and physical characterization of corn stover (Zea mays) for solar biomass pyrolysis potential analysis", ***Bioresource Technology***, Vol. 284, (2019), 466–473. (https://doi.org/10.1016/j.biortech.2019.03.049)

Santos, R. G. dos, and Alencar, A. C.,"Biomass-derived syngas production via gasification process and its catalytic conversion into fuels by Fischer Tropsch synthesis: A review", ***International Journal of Hydrogen Energy***, (2019). (https://doi.org/10.1016/j.ijhydene.2019.07.133)

Santos, V. O., Queiroz, L. S., Araujo, R. O., Ribeiro, F. C. P., Guimarães, M. N., Da Costa, C. E. F., Chaar, J. S., and De Souza, L. K. C.,"Pyrolysis of acai seed biomass : Kinetics and thermodynamic parameters using thermogravimetric analysis", ***Bioresource Technology Reports***, Vol. *12*, (2020), 100553. (https://doi.org/10.1016/j.biteb.2020.100553)

Sarkar, M., Kumar, A., Tumuluru, J. S., Patil, K. N., and Bellmer, D. D.,"Gasification performance of switchgrass pretreated with torrefaction and densification", ***Applied Energy***, Vol. *127*, (2014), 194–201. (https://doi.org/10.1016/j.apenergy.2014.04.027)

Sikarwar, V. S., Zhao, M., Clough, P., Yao, J., Zhong, X., Memon, M. Z., Shah, N., Anthony, E. J., and Fennell, P. S., "An overview of advances in biomass gasification", ***Energy & Environmental Science***, (2016). (https://doi.org/10.1039/C6EE00935B)

Virmond, E., Rocha, J. D., Moreira, R. F. P. M. P. M., José, H. J., and Jose, H. J., "Valorization of agroindustrial solid residues and residues from biofuel production chains by thermochemical conversion: A review, citing brazil as a case study", ***Brazilian Journal of Chemical Engineering,*** Vol. 30, No. 2, (2013), 197–229. (https://doi.org/10.1590/S0104-66322013000200001

Wnorowska, J., Ciukaj, S., and Kalisz, S.,"Thermogravimetric Analysis of Solid Biofuels with Additive under Air Atmosphere", ***Energies***, Vol. 14, (2021), 2257.(https://doi.org/10.3390/en14082257)

Yuan, T., He, W., Yin, G., and Xu, S.,"Comparison of bio-chars formation derived from fast and slow pyrolysis of walnut shell", ***Fuel***, Vol. 261, (2020), 116450. (https://doi.org/10.1016/j.fuel.2019.116450)

Zecca, A., and Chiari, L.,"Fossil-fuel constraints on global warming", ***Energy Policy***, Vol. 38 No. 1, (2010), 1–3. (https://doi.org/10.1016/j.enpol.2009.06.068)

Zhang, J., and Zhang, X., "The thermochemical conversion of biomass into biofuels", ***Biomass, Biopolymer-Based Materials, and Bioenergy***, (2019), 327–368. (https://doi.org/10.1016/b978-0-08-102426-3.00015-1)

Zhou, Q., Cai, W., Zhang, Y., Liu, J., Yuan, L., Yu, F., Wang, X., and Liu, M.,

"Electricity generation from corn cob char through a direct carbon solid oxide fuel cell", ***Biomass and Bioenergy***, Vol. 91, (2016), 250–258. (https://doi.org/10.1016/j.biombioe.2016.05.036)

1.